

Crafting Distribution Shifts for Validation and Training in Single Source Domain Generalization

Nikos Efthymiadis Giorgos Toliadis Ondřej Chum
VRG, Faculty of Electrical Engineering, Czech Technical University in Prague
efthynik@fel.cvut.cz toliageo@fel.cvut.cz chum@cmp.felk.cvut.cz

Abstract

Single-source domain generalization attempts to learn a model on a source domain and deploy it to unseen target domains. Limiting access only to source domain data imposes two key challenges – how to train a model that can generalize and how to verify that it does. The standard practice of validation on the training distribution does not accurately reflect the model’s generalization ability, while validation on the test distribution is a malpractice to avoid. In this work, we construct an independent validation set by transforming source domain images with a comprehensive list of augmentations, covering a broad spectrum of potential distribution shifts in target domains. We demonstrate a high correlation between validation and test performance for multiple methods and across various datasets. The proposed validation achieves a relative accuracy improvement over the standard validation equal to 15.4% or 1.6% when used for method selection or learning rate tuning, respectively.

Furthermore, we introduce a novel family of methods that increase the shape bias through enhanced edge maps. To benefit from the augmentations during training and preserve the independence of the validation set, a k -fold validation process is designed to separate the augmentation types used in training and validation. The method that achieves the best performance on the augmented validation is selected from the proposed family. It achieves state-of-the-art performance on various standard benchmarks. Code at: <https://github.com/NikosEfth/crafting-shifts>

1. Introduction

Visual recognition models are primarily trained using data from one or multiple *source* domains, typically the richest in labeled data or the only available domains during training. The ability of a visual recognition model to generalize or adapt to novel *target* domains with no or limited labeled data is a desirable property. The literature explores such generalization and adaptation under various setups [9, 59]. Supervised domain adaptation refers to cases where labeled

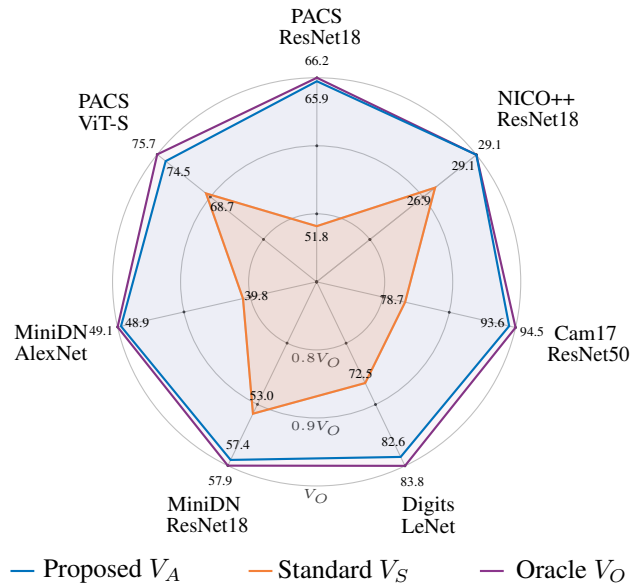


Figure 1. **Test accuracy comparison of different validation methods across seven dataset-backbone configurations.** Each axis ranges from 70% to 100% of the oracle validation V_O that assumes access to the test set. The proposed augmented validation V_A achieves over 98% of the oracle performance on average, representing a 15.4% relevant improvement over the standard validation V_S . For each dataset, the model is chosen from a pool, with 4,500 trained models across all pools.

examples from the target domain are available, while unsupervised domain adaptation deals with unlabeled examples. The task is called domain generalization when there is a complete lack of target domain examples. Depending on whether there is a single or multiple source domains, the task is categorized as single-source domain generalization (SSDG) or multi-source domain generalization (MSDG), respectively.

The lack of labeled target domain examples is a challenging factor for performing both model validation, *i.e.*, estimating a model’s accuracy to tune its hyper-parameters, and method selection, *i.e.*, evaluating which method is the best. This often leads to oracle-based validation, where access to the test set is incorrectly assumed. This aspect

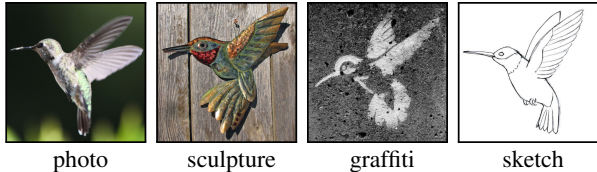


Figure 2. “Hummingbird” in four different domains. The domain generalization task tacitly assumes domains that share informative, human-understandable features, such as texture, shape, or semantics. Therefore, the unseen domains are expected to be human-recognizable. Images from ImageNet [14] and ImageNet-R [27]

is investigated in the work of Musgrave *et al.* [44] for unsupervised domain adaptation and in Gulrajani *et al.* [24] for MSDG, where proper validation protocols are suggested to avoid malpractice. In the context of MSDG, vanilla training on the source domains is top-performing [24] when methods are tested on datasets they were not designed for. Therefore, effective method selection processes are of paramount importance in practice.

In the context of SSDG, developing a visual recognition model robust to unseen distribution shifts during test time is the most challenging of the tasks above. Due to the absence of a proper validation set and protocol, practitioners need to rely on educated guesses to enhance the generalizability of their models. Without an effective validation protocol, it becomes impossible to determine the effectiveness of any model enhancement. To our knowledge, no prior work studies validation protocols in SSDG.

In this work, we follow a fundamental direction in the generalization task, *i.e.*, data augmentations, to synthesize new distributions. The effect of data augmentations is studied extensively in the context of domain generalization, both in combination with adversarial learning [55, 58] and standalone [8, 61]. However, in prior work, augmentations were exclusively used to extend the training set in size and variability. Instead, we apply them to source domain images to obtain a validation set with increased variability and estimate the method’s performance on unseen distributions. We argue that exploiting an exhaustive list of existing augmentations synthesizes instances that span various human-recognizable domains. These augmentations preserve human-recognisable features by their design, while the attempt for completeness ensures the coverage of several unseen potential domains (Figure 2). Since these augmentations are also valuable in the training phase, we propose a k -fold cross-validation scheme performed across augmentation types to get the best of both worlds. This way, the training set is augmented with challenging examples while, at the same time, the validation provides an unbiased estimate of performance on unseen distributions. Using the proposed validation for model selection and hyper-parameter tuning, we achieve better performance than the standard practice on various datasets (see Figure 1).

Besides the novel validation method for SSDG, we propose a family of classification methods parametrized by several train and test-time hyper-parameters. The values of these parameters are selected by the proposed validation method. We focus on enforcing shape bias [19], whose effectiveness is demonstrated in prior work [25, 46, 47]. We accomplish this by using a specialized image transformation technique, employing enhanced edge maps that eliminate textures while retaining crucial shape information. The transformation is performed both during training and testing, with and without randomization, respectively. Despite its simplicity, the proposed method sets a new state-of-the-art on multiple benchmarks, highlighting the value of pronounced shape information and exhaustive augmentations, as well as the effectiveness of the proposed validation (see Figure 4).

2. Related work

We review the prior work on MSDG and SSDG, a less explored task, and discuss shape bias methods in domain generalization and prior work on augmentation strategies.

Multi-source domain generalization. Domain-invariant feature learning is the most popular family of approaches, originating from the results of Ben-David *et al.* [1]: The upper bound of the target domain error is a function of the discriminability between the source and target domain in the feature space. Many follow-up methods exist in the MSDG literature, such as kernel-based approaches [43] or multi-task autoencoders [21]. Ganin *et al.* [18] and Li *et al.* [38] perform adversarial learning to match the domain distributions. Kim *et al.* [30] propose bringing the same-class representations closer regardless of domain. Li *et al.* [37] encourage domain invariance by mixing domain-specific network components with domain-agnostic ones.

The use of data augmentations during training is another common approach. Zhou *et al.* [66] synthesize new examples from pseudo-novel domains conditioned on existing examples while enforcing semantic consistency. Stylization using images from different domains as styles is a simple but effective approach in the work of Somavarapu *et al.* [54], while Mancini *et al.* [41] use mixup [64] to combine different source domains. Carlucci *et al.* [3] additionally optimize the classification loss to train a model that solves jigsaw puzzles in a self-supervised manner. Mansilla *et al.* [42] identify and control domain-specific conflicting gradients.

Regarding generalization in real-world domain shifts, two popular benchmarks exist for MSDG: iWildCam [31] and NICO++ [65]. In iWildCam, a tiny fraction of all classes are seen in each domain, making this benchmark unsuitable for SSDG. NICO++, on the other hand, consists of real photographs taken in different conditions and is suitable for SSDG. We repurpose it for our task to demonstrate that both the proposed method and validation protocol improve under real-world domain shifts.

Single-source domain generalization. Most existing SSDG methods rely on data augmentation or data generation. Volpi *et al.* [55] generate hard examples from an imaginary target domain, while Yue *et al.* [62] use style transfer to produce images of novel styles. Qiao *et al.* [51] use adversarial domain augmentation and an auxiliary Wasserstein auto-encoder to force semantic consistency between the augmented and original images in the latent space. Xu *et al.* [61] propose random convolutions as an augmentation technique to diversify the training data. Wang *et al.* [58] propose a style-complement module to transform training examples in a way that is complementary to the source domain. A Fourier-based augmentation mixing the amplitude of two images is proposed by Xu *et al.* [60], who assume that the Fourier phase is not easily affected by domain shifts. Wan *et al.* [56] target domain invariance through a decomposition and composition technique that builds on the bag-of-words model. Lee *et al.* [34] use a distillation approach by creating an ensemble prediction from images of the same class and penalizing the mismatched outputs with the ensemble. Chen *et al.* [6] propose a center-aware adversarial augmentation that enriches the training samples by pushing them away from the class centers using an angular center loss. Chen *et al.* [5] use a learnable consistency loss for test-time adaptation, and they introduce additional adaptive parameters during the test phase. Chen *et al.* [4] propose a new learning paradigm for training with domain shifts by employing meta-causal learning to simulate a domain shift, analyze its causes, and reduce it. Choi *et al.* [8] enhance the idea of random convolution by recursively stacking ones with small kernel sizes, deformable offsets, and affine transformations.

Shape bias. Geirhos *et al.* [19] show that, in contrast to human subjects, CNNs trained on ImageNet are biased to focus on textures and mitigate that by training on a stylized version of ImageNet. SagNet [45] disentangles style encodings from class categories to prevent style bias and to focus more on object shapes. Edge detection as a bridge between domains has a prominent role, such as in the work of Harary *et al.* [25], who target few-shot learning and rely on domain labels. Another example is the work of Nazari and Kovashka [47], where edge detection forms a fixed augmentation used both for training and testing. Our work has similarities but also differences. Namely, we use improved shape representations, while our method uses a single backbone instead of one backbone for images and one for edge maps. The superiority of this choice is experimentally validated. Narayanan *et al.* [46] argue that the shock graph of the contour map of an image is a complete representation of its shape content. As a drawback, the high cost of their approach does not allow pre-training on ImageNet, and any corresponding performance gain is lost.

Augmentation strategies. Various data augmentation techniques exist to enhance model performance. Com-

mon practices include flipping and cropping [26], occlusion (Cutout) [13], segment replacement (CutMix) [63], or element-wise convex combination of images (Mixup) [64]. Learned approaches, like AutoAugment [10], tune an augmentation set to optimize the performance of downstream tasks. Alternatively, Patch Gaussian [23] applies Gaussian noise to random image portions as an augmentation. AugMix [28] combines randomly generated augmentations while ensuring consistency through a Jensen-Shannon loss. In this work, we randomly sample augmentations from a single library to avoid introducing bias by tailoring the selection to specific datasets. Nevertheless, the above strategies can be orthogonally used with the proposed augmented validation protocol.

3. Training, validation and testing in SSDG

SSDG training is performed on a source domain, and the model is tested on an unseen target domain. The same categories are to be recognized in both source and target domains, *i.e.*, the label spaces are identical. The input space of the source and target domain are RGB images, but their distributions differ. The goal is to perform training so the model can generalize to the target domain. A validation set is necessary but can only be constructed from images of the source domain. Nevertheless, using the raw images is unlikely to reflect any generalization ability in the validation.

To evaluate the generalization capabilities of a model, we introduce the concept of an augmented validation set. In contrast to the well-established practice of using a small set of domain-appropriate augmentations to training images, a wide range of augmentations are drawn from an exhaustive list of existing techniques. This validation set is used in conjunction with the proposed SSDG method, whose key component is the direct injection of shape information in the training procedure. The augmentations used for the validation set are also optionally used in the training. In that case, a two-fold cross-validation process over the augmentation groups is proposed to ensure the validation is performed on a previously unseen distribution.

During the testing phase, two possible approaches are explored. The first performs classification on the input image alone. The second leverages both the input image and its corresponding shape information – the weighted average of the predictions from both inputs is used (see Figure 3).

3.1. Proposed validation set

Motivation: Proper validation is crucial for effective model selection and hyperparameter tuning in any machine learning task, including SSDG. In the context of SSDG, the standard practice is to employ a validation set from raw images of the source domain. However, this validation set alone cannot accurately reflect the model’s generalization performance across other domains. As a result, methods that perform

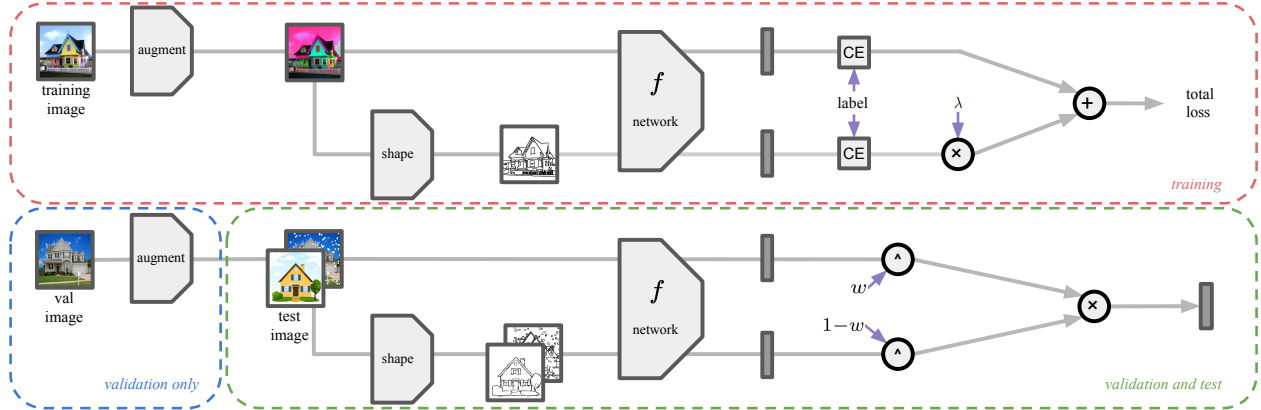


Figure 3. **Overview of the training, validation, and testing pipeline.** Training images are augmented with *basic* and a sub-set of *extra* augmentations. The shape information, encoded as binary thin edges of the augmented image, generates an additional training example. The contribution of the two losses, image and shape-based, is weighed by a parameter λ . In validation, extra augmentations that were not included in the training are used to synthesize unseen distributions. The shape information is optionally exploited in testing and in the validation phase. The final prediction is obtained by ensembling the image and the shape-based predictions, weighted by a parameter w .

well in the source domain are favored by such a process. We introduce a synthetic distribution shift by manipulating the validation set of the source domain to evaluate performance under a distribution shift. This allows us to emulate the challenges posed by domain shifts and obtain a more realistic assessment of the model’s generalization capabilities. To capture the generalization performance across multiple domains, we heavily rely on existing image augmentations. Specifically, we incorporate a wide range of diverse augmentations into our approach, aiming to cover as many variations as possible.

Variants: The following constructions of the validation set are considered and compared.

- **Oracle** - V_O : The *Oracle validation set* is equivalent to the test set. In the case of multiple test sets, their union is considered. In this work, oracle validation is **never** used to compare performance with prior approaches. It is only used as an upper bound on method performance and to measure how close the results achieved with the proposed validation set/method are to the best possible.
- **Standard** - V_S : This validation set consists of raw images from the source domain. In this case, there is no distribution shift between the training and validation sets. It is also referred to as the *standard validation set* and is equivalent to validation on the training distribution.
- **Augmented** - V_A : A total of 76 different augmentations organized into 10 groups according to their types are used to alter the images. Each image in the standard validation set V_S is augmented 10 times by one random augmentation per group, resulting in a validation set 10 times larger than V_S . This *augmented validation set* is created once. The same set is used in all experiments for V_A . The `ImgAug`¹ library is utilized with all its implemented

augmentations and category groups. We refer to these as *extra augmentations* to differentiate them from the *basic augmentations* (random crop, scale, and flip).

3.2. Proposed recognition method

Motivation: The proposed family of methods builds upon previous findings that highlight the texture bias in CNNs [19]. Since CNNs primarily capture texture cues during the training, their performance tends to suffer when confronted with domains lacking these texture cues. To address this limitation, we introduce an explicit enhancement of the shape bias by incorporating shape information extracted from the images in the form of edges. Shape is a fundamental characteristic across multiple domains, making it valuable for bridging the domain gap. By using edge detection, we enable the mapping of objects to a common domain. The shape information is used both during training and testing to reinforce this bridging effect. The parameters mixing the image and shape information are tuned according to the augmented validation.

We additionally investigate the effect of using the extra augmentations during training. Overlap between training and validation distributions may result in overestimating the expected performance due to validation on a seen distribution. To avoid this, the training and validation augmentation groups are kept disjointed via a two-fold validation process. **Network architecture:** A standard backbone taking an RGB image as input followed by a linear classifier providing a class probability at the output is employed. In our experiments, AlexNet [32], ResNet [26], and ViT [15] are used.

Shape extraction: To obtain an explicit shape representation, a modified version of the binary thin edges (BTE) [16] is used. BTE maps the input image to a binary edge map. Edges are extracted by the Sobel operator instead of the learned edge detectors used in [16]. Detected edges are

¹<https://github.com/aleju/imgaug>

further processed by thinning, hysteresis with an adaptive threshold, and removing small connected components. During training, shape variation is achieved with randomized geometric augmentation and randomization of the thresholding process. Binarization provides a form of cleaning shape-irrelevant information, typically corresponding to background.

Training augmentations: *Basic augmentations* (random crop, scale, and flip) are used in all our experiments. When the *extra augmentations* are used in training, each input image is transformed with at most one randomly sampled extra augmentation performed before the basic augmentations.

Training variants: A family of methods is proposed and experimentally evaluated. The network is always trained with cross-entropy loss, while the network input during the training phase varies.

- I : Training baseline - training is performed on images of the source domain.
- \hat{I} : Training is performed on images of the source domain with extra augmentations.
- S : Training is performed with shape information only. Shape is captured in the form of BTEs obtained from images of the source domain.
- IS : Training is performed with both images of the source domain and their BTEs. The loss on the image ℓ_I and the loss on the shape information ℓ_S are combined by $\ell_I + \lambda\ell_S$. Unless otherwise stated, the two losses are balanced by $\lambda = 1.0$.
- $\hat{I}S$: Same as the above but with extra augmentations applied to the input images.
- $IS_{\times 2}$: Same as IS but with two separate backbones for images and BTEs.

Testing variants: The following variants of the network input during test time are considered.

- I : Testing baseline - testing is performed on the input images of the target domain.
- S : Testing is performed on BTEs of the target domain.
- IS : Testing is performed on both images and BTEs of the target domain. Let's denote by p_I and p_S the probability of a particular class based on the input image and BTE, respectively. The combined response is given by their geometric mean $p_I^w p_S^{(1-w)}$, with $w \in [0, 1]$. This is a generalized approach that reduces to testing solely on I or S for $w = 1$ or $w = 0$, respectively. When reporting the value of w , we denote this variant by $I^w S$ for brevity.
- $IS_{\times 2}$: Both backbones, each with the corresponding input, are used for testing, which aims to form a more costly approach for the experimental comparisons.

Training-testing combinations: The training-testing combinations are denoted by $A \rightarrow B$ for training with variant A and testing with variant B . The *baseline* method that trains

on source domain images (training baseline) and tests on target domain images (testing baseline) is denoted as $I \rightarrow I$. In principle, all combinations are possible since there is no testing constraint, only on inputs during training. Nevertheless, we mostly focus on the following: $\hat{I} \rightarrow I$, $S \rightarrow S$, $IS \rightarrow IS$, $\hat{I}S \rightarrow IS$, and $IS_{\times 2} \rightarrow IS_{\times 2}$. An overview of our training, validation, and testing process is shown in Figure 3.

Two-fold cross-validation over augmentation groups: Training with the extra augmentations, *i.e.*, \hat{I} variants, which are used for the validation set, also invalidates the concept of validating on unseen distributions. Therefore, we propose a two-fold cross-validation (TCV) protocol. That is, to train using half of the augmentation groups while keeping the rest to create the validation set. This process is repeated twice, once for each half used in training, and the validation performance is the average of the two runs for a particular variant or value of a hyperparameter. During the final stage, the network is trained with the chosen hyper-parameters using all available augmentations.

4. Experiments

4.1. Experimental setup and implementation

The proposed validation and classification methods are evaluated on five datasets, namely Digits [12, 17, 33, 48], PACS [36], Mini-DomainNet [50], NICO++ [65], and Camelyon17 [2]. The classifier performance is measured by *classification accuracy*. Digits is composed of five different datasets, namely MNIST [33], SVHN [48], MNIST- M [17], SYN [17], and USPS [12], each one corresponding to a different domain. PACS is a domain generalization dataset with four domains: photo, art paintings, cartoon, and sketch. Mini-DomainNet is a subset of the domain generalization dataset DomainNet [50]. It consists of four domains: clipart, painting, real, and sketch. NICO++ consists of natural images, with domains defined as the context: autumn, dim light, grass, outdoor, rock, and water. Camelyon17 is a medical tumor detection dataset, and the domains are defined by the five different hospitals that provided the data. We follow the setup of [7] and train on hospitals 1, 2, and 3 without using the domain labels, while we test on hospitals 4 and 5. The source domain is set to be MNIST, *photos*, and *real* for Digits, PACS, and Mini-DomainNet, respectively. We are the first to work on SSDG with NICO++, where we treat each domain as a source domain and the five others as target domains.

We use AlexNet [32], ResNet-18, and ResNet-50 [26] pre-trained on ImageNet-1k [14], and ViT-Small [15] pre-trained first on ImageNet-21k [53] and then on ImageNet-1k. The pre-trained networks justify using only *photos* and *real* as source domains for PACS and Mini-DomainNet; all other options violate the SSDG protocol since two domains are seen during training. On Digits we use a simple LeNet (conv-

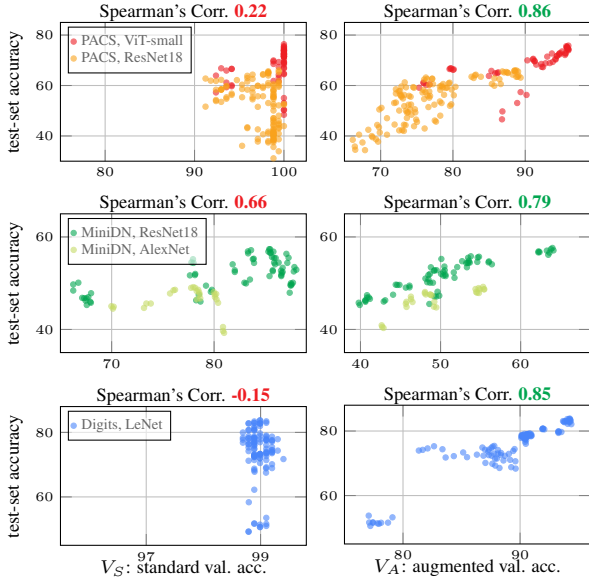


Figure 4. **Correlation between validation and test accuracy across the proposed variants.** Standard validation V_S is performed on the validation set of the source domain, while the proposed augmented validation V_A uses images alternated by augmentations unseen during training. Each point represents a different training-testing model variant.

relu-pool-conv-relu-pool) architecture [3, 55]. On NICO++, following the dataset guidelines, we start with a randomly initialized ResNet-18. Implementation details are included in the Appendix.

4.2. Prior methods

Publicly available implementations of SelfReg [30], SagNet [45], L2D [58], and ACVC [11] are used for the comparison of our method with the state-of-the-art. These methods are also used to demonstrate the effectiveness of the proposed validation set on method selection. Implementation details regarding those methods are included in the Appendix.

4.3. Results

We perform two types of experiments: (i) to show the effectiveness of the proposed validation method, and (ii) to compare the proposed family of approaches with the state-of-the-art. Our main variant is $\hat{I}S \rightarrow I^{.75}S$, given that it is the top performing and is the most frequently selected by our validation method.

Correlation of validation and test performance. The models of the *proposed variants* are evaluated on the standard validation set V_S , the proposed augmented validation V_A , and the test data. To visualize the reliability of predictions based on validation set performance, scatter plots comparing validation versus test performance are shown in Figure 4. Performance on the proposed V_A shows a much higher correlation with the test performance. The performance saturation on V_S for simple tasks like PACS is a major issue.

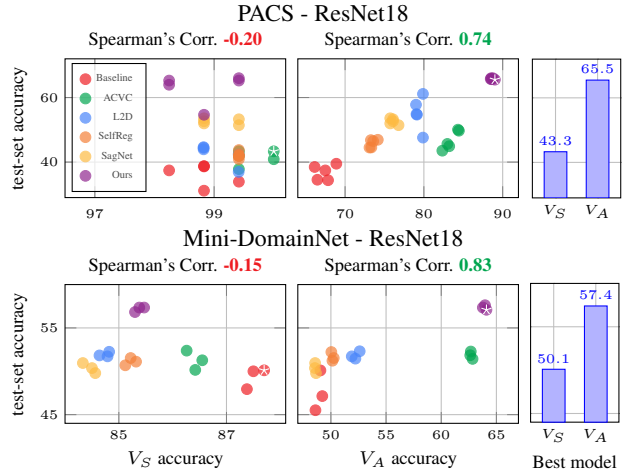


Figure 5. **Correlation between validation and test accuracy across literature methods** and our main variant $\hat{I}S \rightarrow I^{.75}S$ using standard V_S and augmented V_A validation set. The best model, according to each validation performance, is marked with a star. The test performance of the best model per validation set is summarized in the bar plot. V_A achieves significant test accuracy improvements of 22.2 in PACS and 7.3 in Mini-DomainNet.

A similar scatter plot for *prior methods, the baseline, and our main variant* $\hat{I}S \rightarrow I^{.75}S$ is shown in Figure 5. Again, V_A delivers better test performance prediction than V_S . V_S shows a weak negative correlation with the test performance and predicts that most existing methods, including ours, will not surpass the baseline. As such, these methods would never be applied to the target domain in the real world, and we would never know that they work. V_A , on the other hand, achieves a strong positive correlation with the test set. The gains in test accuracy of using V_A over V_S are clearer in the bar plots (right). The performance of ACVC is over-estimated by V_A ; we speculate this is because the ACVC training uses some of the extra augmentations included in V_A . Although we have not modified the ACVC method to fix this issue, the proposed TCV protocol is applicable.

We perform an experiment to highlight the importance of the *TCV protocol*, *i.e.*, avoiding training and validating on the same pool of augmentations. Figure 6 shows the correlation of the V_A validation with the test performance, with and without TCV. Skipping TCV leads to performance over-estimation for methods that use the same extra augmentations for both training and validation. This is a similar effect to what is observed with validating on the training distribution in Figure 4.

Performance gains by better validation. We conduct an experiment for *method selection* across seven dataset-backbone configurations. The validation process is responsible for tuning the learning rate and selecting the best method out of our variants. More than 4,500 models are trained for this experiment, which effectively increases to more than 15,000 when combined with our testing variants. The results are summarised in Figure 1. The test accuracy of the models

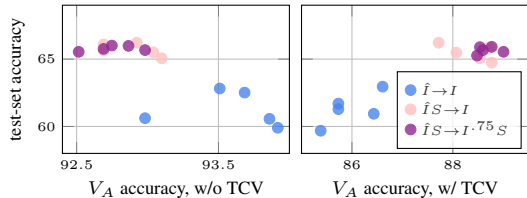


Figure 6. **Correlation between validation and test accuracy with or without TCV** when using V_A as the validation set. The experiment is conducted on PACS using ResNet-18.

selected by V_A significantly surpasses the performance of the ones chosen by V_S for every benchmark. V_A achieves more than 98% of the oracle performance on average.

We perform a hyper-parameter tuning experiment, independently tuning the learning rate and the loss weight λ . We report the performance of the selected models by the two validation processes in Figure 7. The average gain in absolute (relative) test accuracy of V_A compared to V_S is 1.0 (1.6%) for the learning rate and 2.3 (3.9%) for the weight of the loss. Although V_A selects models that perform better in both tuning processes, a higher gain is observed when tuning λ , a hyper-parameter related to domain generalization. On the other hand, the impact of a hyper-parameter related to the learning process, *i.e.*, learning rate, is also expected to be reflected on the validation set from the training distribution. Even in this favorable scenario for V_S , there is no evidence to support using V_S over the proposed V_A .

Impact of components, extra augmentations, and shape usage in training/testing. To study and show the impact of various components of the proposed methods, nine variants are compared in Table 1. The method denoted by S_{sob} uses a non-binarized Sobel edge map instead of BTE, and the method \hat{I}_{+BTE} uses BTE as an additional extra augmentation applied randomly to some images, as opposed to standard input processing applied to all images.

Including shape information during training (var. 2 and 3) gives a noticeable boost in performance across all domains compared to the baseline (var. 1) despite not using shape during testing. Since both images and shapes are processed by the same classifier during training, this is a way to make the network focus on shapes even when the test-time input is only an image. Shape in the form of BTEs (var. 3) contributes much more than the continuous edge maps from the Sobel operator (var. 2), especially in target domains that lack texture information. Additionally, using shape during test time gives a further boost (var. 4). Adding the extra augmentations in training has a positive impact (var. 5 vs. 1, 7 vs. 3, and 8 vs. 4). Using BTE as yet another augmentation type increases the performance (var. 6 vs. 5) but not in the extend of using it on every training image (var. 7 vs. 6) or on test images (var. 8 vs. 6). Lastly, we evaluate the ensemble of two separate networks, one for images and one for shapes. We observe that the single network approach is not only more efficient but also significantly better (var. 9

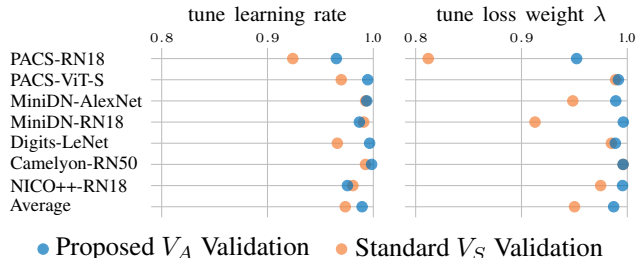


Figure 7. **Learning rate and loss weight tuning per validation.** We fix the training-testing variant to $IS \rightarrow I^{.75}S$ to evaluate the performance of V_A and V_S validation restricted only to hyper-parameter tuning. Performance is normalized by the performance of the oracle; 1 means equivalent to oracle performance.

Variant	Avg.	Art	Cart.	Sketch
1: $I \rightarrow I$ (baseline)	43.46	54.30	37.27	38.80
2: $IS_{sob} \rightarrow I$	51.75	58.35	41.19	55.71
3: $IS \rightarrow I$	57.89	58.47	48.21	67.00
4: $IS \rightarrow I^{.75}S$	59.02	59.10	49.54	68.41
5: $\hat{I} \rightarrow I$	58.15	63.10	48.46	62.91
6: $\hat{I}_{+BTE} \rightarrow I$	59.31	63.38	48.74	65.83
7: $\hat{I}S \rightarrow I$	60.50	63.23	50.62	67.66
8: $\hat{I}S \rightarrow I^{.75}S$	60.97	63.62	50.80	68.50
9: $IS_{\times 2} \rightarrow I^{.75}S_{\times 2}$	53.34	57.52	44.79	57.70

Table 1. **Comparison of variants.** Performance comparison among our variants on the PACS dataset with AlexNet. The value of the shape information and the extra augmentations is showcased. We report accuracy per target domain and their average.

vs. 4). We conclude that it is not only the ensemble of the two predictions that improves the test accuracy but mainly the bridging of the two domains during training.

Beyond shape-oriented domains. PACS and Mini-DomainNet include domains where the shape is preserved, but the texture varies. NICO++ differs because it consists of natural images of objects in varying contexts and environments. We use NICO++ to highlight the generality of the proposed recognition method. Due to the increased experimental cost, we only include the variants $I \rightarrow I$, $IS \rightarrow I^{.75}S$, and $\hat{I}S \rightarrow I^{.75}S$. The baseline $I \rightarrow I$ achieves a 23.8 test accuracy, while including BTEs achieve a 2.2 increase over the baseline, confirming that BTEs not only help the network learn a shape-oriented representation but also enhance robustness against spurious correlations from textures. $\hat{I}S \rightarrow I^{.75}S$ achieves an additional 1.3 increase.

Shape-texture bias. The inductive biases [19] of our approach are analyzed by using the *16-class-ImageNet* [20] as the source domain and the *cue conflict stimuli* images [19] as the target domain. Each stimuli image is the product of blending an image’s texture with another’s shape through style transfer. Therefore, each image has two labels, one based on shape and one based on texture. Although the 16-class-ImageNet consists of 213, 555 images, we sub-sample to 500 images per class. An ImageNet pre-trained ResNet18 backbone is trained with the IS training variant for varying values of the loss weight λ . We compare our variant

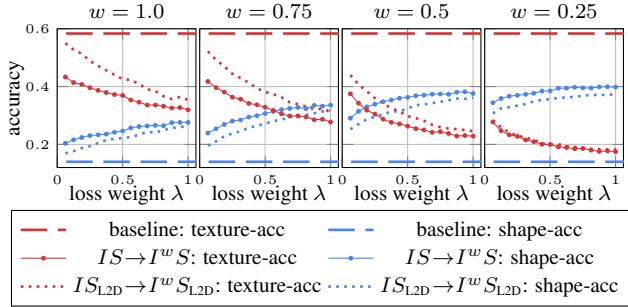


Figure 8. **Shape-texture bias:** The accuracy of different variants is evaluated on the cue conflict stimuli test set based on shape or text labels. Loss weight λ and exponent w are the ways to control the influence of shape during training and testing, respectively, with $\lambda = 1$ and $w = 0$ taking shape into account the most. A different model is trained for the various values of λ .

$IS \rightarrow I^w S$ with a stylization-based approach, a popular shape bias technique. In particular, the style-complement component of L2D [58] is used as a shape component, replacing the BTE. This component is randomized during training and fixed during testing. We refer to this method as $IS_{L2D} \rightarrow I^w S_{L2D}$, and the results are summarized in Figure 8, where accuracy is evaluated either with the shape (shape-acc.) or the texture labels (texture-acc.).

The results demonstrate the significant impact of both shape-controlling hyper-parameters, namely λ during training and w during testing, on shape bias. The comparison shows a higher ability of BTE to adapt to shape cues compared to the stylization of L2D. This seems crucial for domain generalization since humans achieve an accuracy of 95.9 regarding the shape labels [19].

Comparison with the state-of-the-art is presented in Table 2. Whenever available, we include the reported results from the relevant publications. For the experiments on Mini-DomainNet we use the official code of each method. The results reported for our method were obtained by fully automated tuning of the learning rate and method selection among the $\hat{IS} \rightarrow I^w S$ variants on the augmented validation set. *To our knowledge, no previously reported performance has resulted from such a validation process.* State-of-the-art results are achieved on all four datasets.

5. Conclusions

We show that independent augmentations of the validation set allow for better model selection and hyper-parameter tuning in single-source domain generalization. The proposed augmented validation enables the prediction of the test performance for prior methods and the proposed family of methods. Compared to the standard validation practice on the training distribution, the proposed validation method results in significant performance gains in real-world method selection over six domain generalization approaches. We expect this contribution to be valuable for future compar-

Method	SVHN	MNIST-M SYN	USPS	Avg.
ERM [8]	32.52	54.92	42.34	78.21
RandConv [61]	62.07	87.89	63.90	84.39
L2D [58]	62.86	87.30	63.72	83.97
MetaCNN [56]	66.50	88.27	70.66	89.64
MCL [4]	69.94	78.34	78.47	88.54
ProRandC [8]	69.67	82.30	79.77	93.67
CADA [6]	67.27	78.66	79.34	<u>96.96</u>
ABA _{5l} +RC [7]	56.87	80.08	73.40	<u>96.55</u>
$\checkmark IS \rightarrow I^{75} S$ (Ours)	67.82 ± 10	84.28 ± 04	79.64 ± 10	82.61 ± 05

(a) Digits with LeNet.

Method	Clipart	Painting	Sketch	Avg.
ERM [†]	50.53	53.86	38.36	47.58
SagNet [†] [45]	49.63	55.66	45.82	50.37
ACVC [†] [11]	53.81	<u>56.93</u>	43.17	51.27
SelfReg [†] [30]	52.96	53.76	<u>48.25</u>	51.66
L2D [†] [58]	<u>54.95</u>	55.38	45.15	<u>51.83</u>
$\checkmark IS \rightarrow I^{75} S$ (Ours)	55.55 ± 03	59.00 ± 05	57.51 ± 12	57.35 ± 03

(b) Mini-DomainNet with ResNet18.

Alexnet				
Method	P→A	P→C	P→S	Avg.
ERM	54.43	42.74	42.02	46.39
L2D [58]	<u>56.26</u>	51.04	58.42	55.24
MetaCNN [56]	54.05	53.58	63.88	57.17
$\checkmark IS \rightarrow I^{75} S$ (Ours)	63.62 ± 04	50.80 ± 11	68.50 ± 13	60.97 ± 07

ResNet18				
Method	P→A	P→C	P→S	Avg.
ERM	64.10	23.60	29.10	38.90
SagNet [45]	<u>69.80</u>	35.10	40.70	48.50
SelfReg [30]	67.72	28.97	33.71	43.46
XDED [34]	71.40	<u>54.30</u>	51.50	59.10
ITTA [5]	66.50	52.20	<u>63.80</u>	60.80
MCL [4]	-	-	-	59.60
ProRandC [8]	-	-	-	<u>62.89</u>
CADA [6]	-	-	-	56.65
ABA _{5l} [7]	-	-	-	59.04
$\checkmark IS \rightarrow I^{75} S$ (Ours)	67.97 ± 06	54.45 ± 12	74.13 ± 07	65.85 ± 05

(c) PACS.

Method	Hospital 5		Avg.
	Hospital 4	Hospital 5	
ERM	90.58	82.26	86.42
AdvBNN [40]	87.30	80.79	84.04
AugMix [28]	85.92	84.86	85.39
AugMax [57]	79.61	85.51	82.56
RandConv [61]	90.64	84.75	87.70
ABA _{5l} +A [7]	91.85	87.92	89.88
$\checkmark IS \rightarrow I$ (Ours)	<u>92.20 ± 19</u>	<u>94.91 ± 09</u>	<u>93.56 ± 14</u>
$\checkmark IS \rightarrow I^{75} S$ (Ours)	92.88 ± 07	95.86 ± 02	94.37 ± 03

(d) Camelyon17 with ResNet50.

Table 2. Comparison with the state-of-the-art on Digits (a), Mini-DomainNet (b), PACS (c), and Camelyon17 (d). The source domains are MNIST, real, photo, and hospitals 1-3, respectively. Each column represents a different target domain. Methods evaluated by us are denoted with a [†], and the variant of our method chosen by V_A is denoted by \checkmark . ERM corresponds to $I \rightarrow I$.

isons and to help researchers avoid the malpractice of tuning on the test set. We further demonstrate that shape extraction in the form of cleaned edge maps is a solid tool for enforcing shape bias and enhancing the domain generalization ability of deep classifiers. State-of-the-art performance is achieved on several benchmarks by a method selected and with hyper-parameters tuned in a fully automated manner on the augmented validation set.

Acknowledgments: This work was supported by the Junior Star GACR GM 21-28830M, the Czech Technical University in Prague grant No. SGS23/173/OHK3/3T/13, and the CTU institutional support (Future fund). We also thank Nikolaos-Antonios Ypsilantis for the fruitful conversations and insightful discussions.

References

- [1] Shai Ben-David, John Blitzer, Koby Crammer, and Fernando Pereira. Analysis of representations for domain adaptation. In *NeurIPS*, 2007. [2](#)
- [2] Péter Bándi, Oscar Geessink, Quirine Manson, Marcory Van Dijk, Maschenka Balkenhol, Meyke Hermsen, Babak Ehteshami Bejnordi, Byungjae Lee, Kyunghyun Paeng, Aoxiao Zhong, Quanzheng Li, Farhad Ghazvinian Zanjani, Svitlana Zinger, Keisuke Fukuta, Daisuke Komura, Vlado Ovtcharov, Shenghua Cheng, Shaoqun Zeng, Jeppe Thagaard, Anders B. Dahl, Huangjing Lin, Hao Chen, Ludwig Jacobsson, Martin Hedlund, Melih Çetin, Eren Halici, Hunter Jackson, Richard Chen, Fabian Both, Jörg Franke, Heidi Küsters-Vandeveld, Willem Vreuls, Peter Bult, Bram van Ginneken, Jeroen van der Laak, and Geert J. S. Litjens. From detection of individual metastases to classification of lymph node status at the patient level: The camelyon17 challenge. *IEEE Trans. Med. Imaging*, 2019. [5](#)
- [3] Fabio Maria Carlucci, Antonio D’Innocente, Silvia Bucci, Barbara Caputo, and Tatiana Tommasi. Domain generalization by solving jigsaw puzzles. In *CVPR*, 2019. [2](#), [6](#), [12](#)
- [4] Jin Chen, Zhi Gao, Xinxiao Wu, and Jiebo Luo. Meta-causal learning for single domain generalization. In *CVPR*, 2023. [3](#), [8](#), [12](#)
- [5] Liang Chen, Yong Zhang, Yibing Song, Ying Shan, and Lingqiao Liu. Improved test-time adaptation for domain generalization. In *CVPR*, 2023. [3](#), [8](#), [12](#)
- [6] Tianle Chen, Mahsa Baktashmotlagh, Zijian Wang, and Mathieu Salzmann. Center-aware adversarial augmentation for single domain generalization. In *WACV*, 2023. [3](#), [8](#), [12](#)
- [7] Sheng Cheng, Tejas Gokhale, and Yezhou Yang. Adversarial bayesian augmentation for single-source domain generalization. In *ICCV*, 2023. [5](#), [8](#)
- [8] Seokeon Choi, Debasmit Das, Sungha Choi, Seunghan Yang, Hyunsin Park, and Sungrack Yun. Progressive random convolutions for single domain generalization. In *CVPR*, 2023. [2](#), [3](#), [8](#), [12](#)
- [9] Gabriela Csurka. Domain adaptation for visual applications: A comprehensive survey. In *Advances in Computer Vision and Pattern Recognition*, 2017. [1](#)
- [10] Ekin Dogus Cubuk, Barret Zoph, Dandelion Mane, Vijay Vasudevan, and Quoc V. Le. Autoaugment: Learning augmentation policies from data. In *CVPR*, 2019. [3](#)
- [11] Ilke Cugu, Massimiliano Mancini, Yanbei Chen, and Zeynep Akata. Attention consistency on visual corruptions for single-source domain generalization. In *CVPRW*, 2022. [6](#), [8](#)
- [12] John Denker, W. Gardner, Hans Graf, Donnie Henderson, R. Howard, W. Hubbard, L. D. Jackel, Henry Baird, and Isabelle Guyon. Neural network recognizer for hand-written zip code digits. In *NeurIPS*, 1988. [5](#)
- [13] Terrance DeVries and Graham W Taylor. Improved regularization of convolutional neural networks with cutout. *arXiv preprint arXiv:1708.04552*, 2017. [3](#)
- [14] Wei Dong, Richard Socher, Li Li-Jia, Kai Li, and Li Fei-Fei. ImageNet: A large-scale hierarchical image database. In *CVPR*, 2009. [2](#), [5](#)
- [15] Alexey Dosovitskiy, Lucas Beyer, Alexander Kolesnikov, Dirk Weissenborn, Xiaohua Zhai, Thomas Unterthiner, Mostafa Dehghani, Matthias Minderer, Georg Heigold, Sylvain Gelly, Jakob Uszkoreit, and Neil Houlsby. An image is worth 16x16 words: Transformers for image recognition at scale. *ICLR*, 2021. [4](#), [5](#)
- [16] Nikos Efthymiadis, Giorgos Tolias, and Ondrej Chum. Edge augmentation for large-scale sketch recognition without sketches. In *ICPR*, 2022. [4](#), [11](#)
- [17] Yaroslav Ganin and Victor Lempitsky. Unsupervised domain adaptation by backpropagation. In *ICML*, 2015. [5](#)
- [18] Yaroslav Ganin, Evgeniya Ustinova, Hana Ajakan, Pascal Germain, Hugo Larochelle, François Laviolette, Mario Marchand, and Victor Lempitsky. Domain-adversarial training of neural networks. *JMLR*, 2016. [2](#)
- [19] Robert Geirhos, Patricia Rubisch, Claudio Michaelis, Matthias Bethge, Felix A Wichmann, and Wieland Brendel. Imagenet-trained cnns are biased towards texture; increasing shape bias improves accuracy and robustness. In *ICLR*, 2019. [2](#), [3](#), [4](#), [7](#), [8](#), [11](#)
- [20] Robert Geirhos, Carlos R. M. Temme, Jonas Rauber, Heiko H. Schütt, Matthias Bethge, and Felix A. Wichmann. Generalisation in humans and deep neural networks. In *NeurIPS*, 2018. [7](#), [11](#)
- [21] Muhammad Ghifary, W Bastiaan Kleijn, Mengjie Zhang, and David Balduzzi. Domain generalization for object recognition with multi-task autoencoders. In *ICCV*, 2015. [2](#)
- [22] Chris A. Glasbey. An analysis of histogram-based thresholding algorithms. *CVGIP*, 1993. [12](#)
- [23] Raphael Gontijo Lopes, Dong Yin, Ben Poole, Justin Gilmer, and Ekin D. Cubuk. Improving Robustness Without Sacrificing Accuracy with Patch Gaussian Augmentation. In *ICMLW*, 2019. [3](#)
- [24] Ishaan Gulrajani and David Lopez-Paz. In search of lost domain generalization. In *ICLR*, 2021. [2](#)
- [25] Sivan Harary, Eli Schwartz, Assaf Arbel, Peter Staar, Shady Abu-Hussein, Elad Amrani, Roei Herzig, Amit Alfassy, Raja Giryes, Hilde Kuehne, et al. Unsupervised domain generalization by learning a bridge across domains. In *CVPR*, 2022. [2](#), [3](#)
- [26] Kaiming He, Xiangyu Zhang, Shaoqing Ren, and Jian Sun. Deep residual learning for image recognition. In *CVPR*, 2016. [3](#), [4](#), [5](#)
- [27] Dan Hendrycks, Steven Basart, Norman Mu, Saurav Kadavath, Frank Wang, Evan Dorundo, Rahul Desai, Tyler Lixuan Zhu, Samyak Parajuli, Mike Guo, Dawn Xiaodong Song, Jacob Steinhardt, and Justin Gilmer. The many faces of robustness: A critical analysis of out-of-distribution generalization. *ICCV*, 2020. [2](#)
- [28] Dan Hendrycks, Norman Mu, Ekin Dogus Cubuk, Barret Zoph, Justin Gilmer, and Balaji Lakshminarayanan. Augmix: A simple method to improve robustness and uncertainty under data shift. In *ICLR*, 2020. [3](#), [8](#)
- [29] Yen Jui-Cheng, Chang Fu-Juay, and Chang Shyang. A new criterion for automatic multilevel thresholding. *IEEE Transactions on Image Processing*, 1995. [12](#)
- [30] Daehee Kim, Seunghyun Park, Jinkyu Kim, and Jaekoo Lee. Selfreg: Self-supervised contrastive regularization for domain generalization. In *ICCV*, 2021. [2](#), [6](#), [8](#), [12](#)
- [31] Pang Wei Koh, Shiori Sagawa, Henrik Marklund, Sang Michael Xie, Marvin Zhang, Akshay Balsubramani,

- Weihua Hu, Michihiro Yasunaga, Richard Lanus Phillips, Irena Gao, Tony Lee, Etienne David, Ian Stavness, Wei Guo, Berton A. Earnshaw, Imran S. Haque, Sara Beery, Jure Leskovec, Anshul Kundaje, Emma Pierson, Sergey Levine, Chelsea Finn, and Percy Liang. WILDS: A benchmark of in-the-wild distribution shifts. In *ICML*, 2021. 2
- [32] Alex Krizhevsky, Ilya Sutskever, and Geoffrey E Hinton. Imagenet classification with deep convolutional neural networks. In *NeurIPS*, 2012. 4, 5
- [33] Yann LeCun, Léon Bottou, Yoshua Bengio, and Patrick Haffner. Gradient-based learning applied to document recognition. In *Proceedings of the IEEE*, 1998. 5
- [34] Kyungmoon Lee, Sungyeon Kim, and Suha Kwak. Cross-domain ensemble distillation for domain generalization. In *ECCV*, 2022. 3, 8, 12
- [35] Chun Hung Li and CK Lee. Minimum cross entropy thresholding. *Pattern Recognition*, 1993. 12
- [36] Da Li, Yongxin Yang, Yi-Zhe Song, and Timothy Hospedales. Deeper, broader and artier domain generalization. In *ICCV*, 2017. 5
- [37] D. Li, J. Zhang, Y. Yang, C. Liu, Y. Song, and T. Hospedales. Episodic training for domain generalization. In *ICCV*, 2019. 2
- [38] Ya Li, Xinmei Tian, Mingming Gong, Yajing Liu, Tongliang Liu, Kun Zhang, and Dacheng Tao. Deep domain generalization via conditional invariant adversarial networks. In *ECCV*, September 2018. 2
- [39] Xiao-Chang Liu, Yong-Liang Yang, and Peter Hall. Geometric and textural augmentation for domain gap reduction. In *CVPR*, 2022. 12
- [40] Aleksander Madry, Aleksandar Makelov, Ludwig Schmidt, Dimitris Tsipras, and Adrian Vladu. Towards deep learning models resistant to adversarial attacks. In *ICLR*, 2018. 8
- [41] Massimiliano Mancini, Zeynep Akata, Elisa Ricci, and Barbara Caputo. Towards recognizing unseen categories in unseen domains. In *ECCV*, 2020. 2
- [42] Lucas Mansilla, Rodrigo Echeveste, Diego H Milone, and Enzo Ferrante. Domain generalization via gradient surgery. In *ICCV*, 2021. 2
- [43] Krikamol Muandet, David Balduzzi, and Bernhard Schölkopf. Domain generalization via invariant feature representation. In *ICML*, 2013. 2
- [44] Kevin Musgrave, Serge J. Belongie, and Ser-Nam Lim. Unsupervised domain adaptation: A reality check. In *arXiv*, 2021. 2
- [45] Hyeonseob Nam, HyunJae Lee, Jongchan Park, Wonjun Yoon, and Donggeun Yoo. Reducing domain gap by reducing style bias. In *CVPR*, 2021. 3, 6, 8, 12
- [46] Maruthi Narayanan, Vickram Rajendran, and Benjamin Kimia. Shape-biased domain generalization via shock graph embeddings. In *ICCV*, 2021. 2, 3
- [47] Narges Honarvar Nazari and Adriana Kovashka. The role of shape for domain generalization on sparsely-textured images. In *CVPRW*, 2022. 2, 3
- [48] Yuval Netzer, Tao Wang, Adam Coates, Alessandro Bissacco, Bo Wu, and Andrew Y. Ng. Reading digits in natural images with unsupervised feature learning. *NeurIPSW*, 2011. 5
- [49] Nobuyuki Otsu. A threshold selection method from gray-level histograms. *IEEE Transactions on Systems, Man, and Cybernetics*, 1979. 12
- [50] Xingchao Peng, Qinxun Bai, Xide Xia, Zijun Huang, Kate Saenko, and Bo Wang. Moment matching for multi-source domain adaptation. In *ICCV*, 2019. 5, 11
- [51] Fengchun Qiao, Long Zhao, and Xi Peng. Learning to learn single domain generalization. In *CVPR*, 2020. 3
- [52] T. W. Ridler and S. Calvard. Picture thresholding using an iterative selection method. *Transactions on Systems, Man, and Cybernetics*, 1978. 12
- [53] Tal Ridnik, Emanuel Ben-Baruch, Asaf Noy, and Lih Zelnik-Manor. Imagenet-21k pretraining for the masses. In *NeurIPS*, 2021. 5
- [54] Nathan Somavarapu, Chih-Yao Ma, and Zsolt Kira. Frustratingly simple domain generalization via image stylization. In *arXiv*, 2020. 2
- [55] Riccardo Volpi, Hongseok Namkoong, Ozan Sener, John Duchi, Vittorio Murino, and Silvio Savarese. Generalizing to unseen domains via adversarial data augmentation. In *NeurIPS*, 2018. 2, 3, 6, 12
- [56] Chaoqun Wan, Xu Shen, Yonggang Zhang, Zhiheng Yin, Xinmei Tian, Feng Gao, Jianqiang Huang, and Xian-Sheng Hua. Meta convolutional neural networks for single domain generalization. In *CVPR*, 2022. 3, 8
- [57] Haotao Wang, Chaowei Xiao, Jean Kossaiji, Zhiding Yu, Anima Anandkumar, and Zhangyang Wang. Augmax: Adversarial composition of random augmentations for robust training. In *NeurIPS*, 2021. 8
- [58] Zijian Wang, Yadan Luo, Ruihong Qiu, Zi Huang, and Mahsa Baktashmotlagh. Learning to diversify for single domain generalization. In *ICCV*, 2021. 2, 3, 6, 8, 12
- [59] Karl Weiss, Taghi M Khoshgoftaar, and DingDing Wang. A survey of transfer learning. *Journal of Big data*, 2016. 1
- [60] Qinwei Xu, Ruipeng Zhang, Ya Zhang, Yanfeng Wang, and Qi Tian. A fourier-based framework for domain generalization. In *CVPR*, 2021. 3
- [61] Zhenlin Xu, Deyi Liu, Junlin Yang, Colin Raffel, and Marc Niethammer. Robust and generalizable visual representation learning via random convolutions. In *ICLR*, 2021. 2, 3, 8
- [62] Xiangyu Yue, Yang Zhang, Sicheng Zhao, Alberto Sangiovanni-Vincentelli, Kurt Keutzer, and Boqing Gong. Domain randomization and pyramid consistency: Simulation-to-real generalization without accessing target domain data. In *ICCV*, 2019. 3
- [63] Sangdoon Yun, Dongyoon Han, Sanghyuk Chun, Seong Joon Oh, Youngjoon Yoo, and Junsuk Choe. Cutmix: Regularization strategy to train strong classifiers with localizable features. In *ICCV*, 2019. 3
- [64] Hongyi Zhang, Moustapha Cisse, Yann N Dauphin, and David Lopez-Paz. mixup: Beyond empirical risk minimization. In *ICML*, 2018. 2, 3
- [65] Xingxuan Zhang, Yue He, Renzhe Xu, Han Yu, Zheyang Shen, and Peng Cui. Nico++: Towards better benchmarking for domain generalization. In *CVPR*, 2023. 2, 5
- [66] Kaiyang Zhou, Yongxin Yang, Timothy Hospedales, and Tao Xiang. Learning to generate novel domains for domain generalization. In *ECCV*, 2020. 2

A. Appendix

In this appendix, we provide additional information about the datasets used and implementation details both for the proposed and the literature methods utilized in our experiments. Additionally, we present qualitative examples of the data augmentations and the shape extraction processes used in this work. Finally, we include additional experimental results that could not fit in the main paper, along with tables containing the numerical data of our figures.

A.1. Dataset Details

Digits dataset details. It is a collection of five digit-recognition datasets: MNIST, MNIST-M, SVHN, SYN, and USPS. MNIST-M combines the original MNIST handwritten digit database with random patches of the BSDS500 dataset. SVHN is a dataset of real-world house number images obtained by Google Street View. SYN is a synthetic dataset created from different Windows fonts after applying geometric transformations and blurring. USPS is a dataset of scanned digits from U.S. Postal Service envelopes. To compare with the literature, we use only the first 10,000 images of the MNIST training set. We choose to use the 90% for training and the 10% for validation. We are evaluating on the test set of the rest domains.

PACS dataset details. It is a domain generalization dataset that includes four domains: photo, art paintings, cartoon, and sketch. It consists of seven classes and 9,991 images. In the experiments presented in the main paper, the photo domain is used as the source, and the remaining domains are used for evaluation. This appendix provides an additional experiment where each domain is used as the source. The photo domain consists of 1,670 images. We use the official partition of 10% for validation and the rest 90% for training.

Mini-DomainNet dataset details. It is a subset of the domain generalization dataset DomainNet [50]. It consists of 140,006 images, 126 classes, and four domains: clipart, painting, real, and sketch. We use the real domain as the source, and we evaluate on the rest. The real domain has 64,979 images and we are using the official split that includes 58,482 images for training and 6,497 images for validation.

NICO++ dataset details. It is an out-of-distribution generalization dataset comprising natural images, where the following contexts serve as the domains: autumn, dim light, grass, outdoor, rock, and water. NICO++ consists of 60 classes and 88,866 images.

Camelyon17 dataset details. It is a medical dataset focused on tumor detection, with data from five different hospitals. Data from hospitals 1, 2, and 3 are treated as the source domain, and data from hospitals 4 and 5 are the target. Camelyon17 consists of two classes: cancerous and non-cancerous tissue, and it contains 455,954 images.

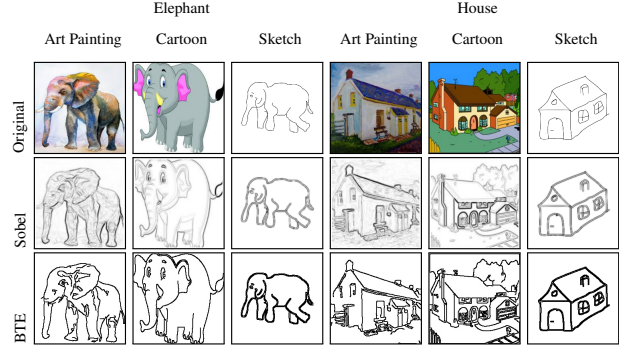


Figure 9. The output of the shape extraction process for BTE and Sobel-based edge maps from the different target domains in the PACS dataset. BTE removes texture cues more effectively, making it a better choice for increasing the shape bias.

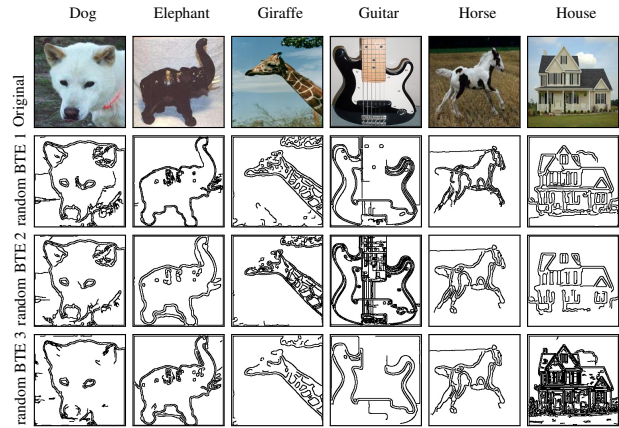


Figure 10. The output of the shape extraction process for BTE edge maps on images of the photo domain in PACS during training. BTE introduces randomization at multiple steps of edge detection, enriching the training set with edge maps that vary in level of detail.

16-class-ImageNet dataset details. The 16-class-ImageNet dataset [20] is a subset of the ImageNet dataset that maps 231 of the original classes to 16 new ones, closer to the level of abstraction a human could guess. Although the 16-class-ImageNet consists of 213,555 images, we sub-sample to 500 images per class. We test the trained models to the texture-shape cue conflict stimuli dataset [19], which is a dataset that shares the same 16 classes and consists of 1,280 images.

A.2. Implementation Details

Shape extraction. The pipeline for BTEs and their randomization is adopted from [16] with the exception that we use Sobel instead of the learnable edge detectors, eliminating the need for additional training data. The pipeline is as follows: First, the image is blurred using a Gaussian filter with kernel size 5 and sigma equal to 1.0. Next, the Sobel operator is applied for edge detection, followed by non-maximum suppression to thin the edge map. Finally, the edge map is

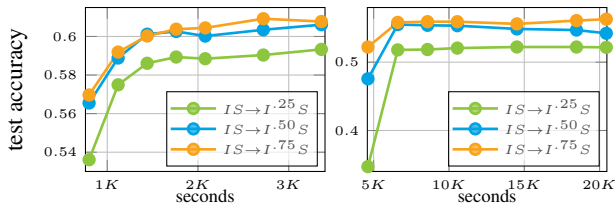


Figure 11. **Accuracy vs Time:** Training on PACS (left) and on Mini-DomainNet (right) with different number of BTEs in the batch. The training batch includes 64 RGB images plus 0, 8, 16, 24, 32, 48, and 64 BTEs (dots).

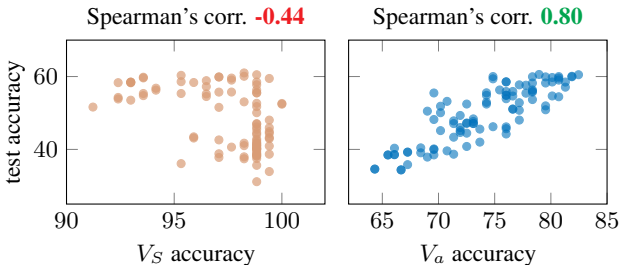


Figure 12. **Augmented validation without increasing the validation set size:** Correlation between the validation and test accuracy using the standard validation and the augmented one of the same size. This experiment shows that it is not the larger size of V_A that makes the difference. The experiment is on the PACS dataset with a ResNet-18 as a backbone.

binarized using adaptive hysteresis. The upper and lower bounds of hysteresis are chosen as $1.5t$ and $0.5t$, respectively, where the threshold t is selected using Otsu’s method on the edge map before thinning.

In the randomized variant used for training, the standard deviation of the Gaussian blurring is chosen randomly from 0, 1, and 2, with 0 corresponding to no blur. The thresholding method is randomly picked among Yen [29], Otsu [49], Isodata [52], Li [35], and the mean method [22]. Additional random noise is introduced in both the threshold value t and the hysteresis bounds, enriching the training set.

In the variant using Sobel edge maps of Table 1, the process is simplified in blurring and applying the Sobel operator. Randomization is only through the standard deviation of the Gaussian blurring. Examples of Sobel-based edge maps and BTEs are shown in Figures 9 and 10.

Implementation details for our approach. The *basic augmentations* include cropping with relative size in $[0.8, 1.0]$, an aspect ratio in $[\frac{3}{4}, \frac{4}{3}]$, resizing to 224×224 , and horizontal flipping with a probability of 0.5. Digits is an exception where the resize is 32×32 , and the flipping is skipped as it conflicts with the task. The *extra augmentations* from the ImgAug library are from the following groups: arithmetic, artistic, blur, color, contrast, convolutional, edges, geometric, segmentation, and weather.

For our PACS, Digits, and Mini-DomainNet experiments, the *learning rate* is tuned using a grid search among 33

Method	Art	Cartoon	Photo	Sketch	Avg.
ERM	68.80	70.00	38.90	39.40	54.30
JiGen [3]	67.70	72.23	41.70	36.83	54.60
ADA [55]	72.43	71.97	44.63	45.73	58.70
SelfReg [30]	72.59	76.56	43.46	45.76	59.59
SagNet [45]	73.20	75.67	48.53	50.07	61.90
GeoTexAug [39]	72.07	78.70	49.07	59.97	65.00
L2D [58]	76.91	77.88	52.29	53.66	65.18
XDED [34]	76.50	77.20	59.10	53.10	66.50
CADA [6]	76.33	79.08	61.59	56.65	68.41
ITTA [5]	74.60	77.10	60.80	61.20	68.40
ProRandC [8]	76.98	78.54	<u>62.89</u>	57.11	68.88
MCL [4]	<u>77.13</u>	80.14	62.55	<u>59.60</u>	<u>69.86</u>
ABA _{sl}	75.34	77.49	58.86	53.76	66.36
$IS \rightarrow I^{.75}S$ (Ours)	80.67 ± 0.4	76.53 ± 1.1	65.85 ± 0.5	58.41 ± 1.3	70.37 ± 0.5

Table 3. **Comparison with state-of-the-art approaches on PACS with a ResNet18 backbone.** Each column corresponds to a different source domain, reporting average performance when testing on the three remaining domains as target domains.

equidistant values on a logarithmic scale in the range of $[10^{-5}, 1]$. The *loss weight* λ is tuned using a grid search among 17 equidistant values in $[0, 1]$. The *exponent* w is a test-time parameter, and it is tuned among the values 0, 0.25, 0.5, 0.75, and 1.0 for all of our experiments. The first and last values correspond to the variants S and I , respectively. Experiments on PACS and Digits for the comparison with the state-of-the-art are repeated 30 times. In all other experiments on PACS, Digits, and Mini-DomainNet, we use 5, 5, and 3 seeds, respectively.

Camelyon17 and NICO++ require longer training because of the larger size of the former and the randomly initialized training of the latter. Therefore, we perform a learning rate grid search for 9 equidistant values on a logarithmic scale, in the range of $[10^{-5}, 1]$, while we train for 3 different seeds.

For the 16-class-ImageNet experiment, we perform a grid search for our IS method’s loss weight λ for 16 different values in the range of $[0.0625, 1]$.

We always use stochastic gradient descent with an exponential scheduler that decreases the learning rate by two magnitudes by the end of the training. We tune the number of epochs and the learning rate jointly for the $IS \rightarrow IS$ variant. This experiment provides us with the number of epochs to use for all variants, which remains fixed for all the follow-up experiments described in the main paper. We train our models for 10, 40, 50, 300, 300, and 700 epochs on Camelyon17, Mini-DomainNet, 16-class-ImageNet, Digits, PACS, and NICO++ respectively.

Implementation details for the literature methods. Regarding SelfReg, SagNet, L2D, and ACVC, we follow all the implementation details – optimizer, schedulers, augmentations, and hyperparameters – from the original works, except for the learning rate. To determine the number of training epochs, we first set the learning rate to the value reported in the publication of the respective method and tune the number of epochs to maximize validation accuracy. Ties are resolved by picking the smaller number, while we never go for more

		PACS-ViT-S		PACS-RN18		MiniDN-RN18		MiniDN-Alexnet		NICO++-RN18		Digits-LeNet		Cam17-RN50	
Val	Method	Acc	Method	Acc	Method	Acc	Method	Acc	Method	Acc	Method	Acc	Method	Acc	
V_O	$iS \rightarrow iS$	75.68	$iS \rightarrow I^{75}S$	66.19	$iS \rightarrow I^{75}S$	57.89	$iS \rightarrow I^{75}S$	49.10	$iS \rightarrow I^{75}S$	29.12	$iS \rightarrow I^{50}S$	83.83	$iS \rightarrow I$	94.47	
V_S	$ties^*$	68.70	$iS \times 2 \rightarrow I^{50}S$	51.75	$iS \times 2 \rightarrow I^{75}S$	52.98	$I \rightarrow I$	39.82	$iS \rightarrow I^{75}S$	26.86	$iS_{sub} \rightarrow I$	72.51	$I \rightarrow I$	78.73	
V_A	$iS \rightarrow I^{75}S$	74.48	$iS \rightarrow I^{75}S$	65.85	$iS \rightarrow I^{75}S$	57.35	$iS \rightarrow I^{75}S$	48.85	$iS \rightarrow I^{75}S$	29.12	$iS \rightarrow I^{75}S$	82.61	$iS \rightarrow I$	93.56	
gain		5.78		14.10		4.37		9.03		2.26		10.10		14.83	

Table 4. **Method selection based on the validation set:** Test accuracy is reported after tuning and selecting the best method among all proposed variants according to different validation sets – *i.e.*, oracle, standard, and augmented. The method chosen and the performance gain between the augmented and the standard validation set are reported. In the case of PACS with a ViT-S model, V_S ties across seven variations, so we report the average.

		tune learning rate				tune loss weight λ								
		Train	Test	V_S	V_A	V_O	Gain	V_S	V_A	V_O	Gain			
PACS	RN18	$iS \rightarrow I^{25}S$		58.0	57.6	61.0	-0.4	37.9	56.1	57.7	18.3			
		$iS \rightarrow I^{50}S$		58.0	59.7	61.3	1.7	35.8	57.1	59.4	21.4			
		$iS \rightarrow I^{75}S$		56.7	59.2	61.3	2.5	49.0	57.5	60.4	8.5			
PACS	ViT-S	$iS \rightarrow I^{25}S$		62.6	65.4	65.9	2.8	63.1	64.9	65.2	1.8			
		$iS \rightarrow I^{50}S$		67.4	68.5	69.4	1.1	68.0	68.1	68.9	0.1			
		$iS \rightarrow I^{75}S$		69.4	71.2	71.5	1.8	70.4	70.6	71.2	0.2			
MiniDN	Alexnet	$iS \rightarrow I^{25}S$		45.3	45.5	45.9	0.2	43.6	44.9	45.4	1.3			
		$iS \rightarrow I^{50}S$		46.9	47.5	48.3	0.6	45.9	47.5	47.9	1.6			
		$iS \rightarrow I^{75}S$		47.8	47.8	48.1	0.0	46.1	48.0	48.6	1.9			
MiniDN	RN18	$iS \rightarrow I^{25}S$		51.8	51.6	51.9	-0.2	47.3	50.8	51.0	3.5			
		$iS \rightarrow I^{50}S$		55.0	55.0	55.5	0.1	48.1	53.9	54.6	5.8			
		$iS \rightarrow I^{75}S$		55.5	55.3	56.0	-0.2	50.1	54.7	54.9	4.6			
Digits	LeNet	$iS \rightarrow I^{25}S$		78.0	78.8	78.9	0.8	75.4	76.0	76.8	0.7			
		$iS \rightarrow I^{50}S$		77.8	78.8	79.1	0.9	76.1	76.3	77.2	0.2			
		$iS \rightarrow I^{75}S$		76.2	78.6	78.9	2.4	76.4	76.7	77.6	0.3			
NICO++	RN18	$iS \rightarrow I^{25}S$		23.4	23.2	23.6	-0.2	23.6	23.7	23.8	0.1			
		$iS \rightarrow I^{50}S$		25.8	25.7	26.2	-0.1	26.0	26.5	26.7	0.5			
		$iS \rightarrow I^{75}S$		26.1	26.0	26.6	-0.1	26.2	26.8	26.9	0.6			
Cam17	RN50	$iS \rightarrow I^{25}S$		92.0	92.3	92.4	0.3	92.1	92.2	92.4	0.1			
		$iS \rightarrow I^{50}S$		93.3	93.4	93.9	0.1	93.7	93.7	93.9	0.0			
		$iS \rightarrow I^{75}S$		93.8	94.3	94.5	0.5	94.1	94.1	94.5	0.0			
Avg gain							0.7				3.4			

Table 5. **Learning rate and loss weight tuning per validation:** Test accuracy for our method variants is reported after tuning according to different validation sets – *i.e.*, oracle, standard, and augmented. The performance gain between the augmented versus the standard validation set is also presented. As expected, the method is more effective for tuning hyperparameters related to domain generalization, such as the shape loss weight.

than 800 or 100 epochs on PACS and Mini-DomainNet, respectively. Once the number of epochs is tuned, we tune the learning rate to maximize validation accuracy.

A.3. Extra Experiments

Performance vs Time: For the proposed validation V_A , there is no matter of time-performance trade-off. We argue that the standard validation V_S is completely incapable of predicting test performance in the context of domain generalization. This can be seen from Figure 5: PACS shows an accuracy drop of 22.2 if V_S is used over V_A . Methods that do not use the proposed augmentations in training, such as L2D and SelfReg, do not require the 2-fold cross-validation. In such cases, the time overhead of V_A over V_S is only the performance of a random augmentation. For methods that use augmentations, the extra time compared to V_S is approximately doubled because of the 2-fold cross-validation.

For the proposed recognition method, the performance vs training time trade-off is shown in Figure 11. Even with roughly half of the training time, when only 25% of the batch images have their BTEs (16 BTEs) used, the test accuracy decrease is approximately 1%. The time measurements were conducted on a single Tesla A100 40GB GPU.

V_A vs V_S : Effective because it is larger? The proposed validation method V_A increases the variability in the validation set as well as the size of the validation set by a factor of 10, which is given by the 10 groups of augmentations. To demonstrate that the benefit does not come from the larger validation set, we create an additional set by augmenting each image only once by randomly picking one of the 10 augmentation groups per image. The result is an augmented set of the same size as the original validation set, which we denote as V_a . We perform the same experiments as in Figure 4 for PACS with a ResNet-18, but we exclude all variations that use augmentations during training to avoid overestimation, as described in Figure 6. Figure 12 shows that validation V_a is still significantly better than V_S .

Experiments with each domain as the source domain. In Table 3 we report the performance on the PACS dataset while using each domain as the source domain. We consider this an invalid setup due to the ImageNet pre-training. The networks have seen both real images during the pre-training phase and also cartoons, artworks, or sketches during training, making it similar to an MSDG task. Additionally, evaluating on the photo domain no longer corresponds to testing on an unseen domain. Nevertheless, we report results following the example of the literature, and our method is, on average, the top performing. Training from scratch would make these setups valid for SSDG, but the literature lacks available results for comparison.

Method selection and hyperparameter tuning. We summarize the results of our experiments for method selection in Table 4 and for hyperparameter tuning in Table 5. These tables contain the data presented in Figure 1 and Figure 7, respectively. While Figure 7 includes only experiments with the variant $iS \rightarrow I^{75}S$, Table 5 also contains the variants $iS \rightarrow I^{25}S$ and $iS \rightarrow I^{50}S$.

Extra augmentations: Examples from the PACS dataset of all 76 extra augmentations are shown in Figures 13-15.

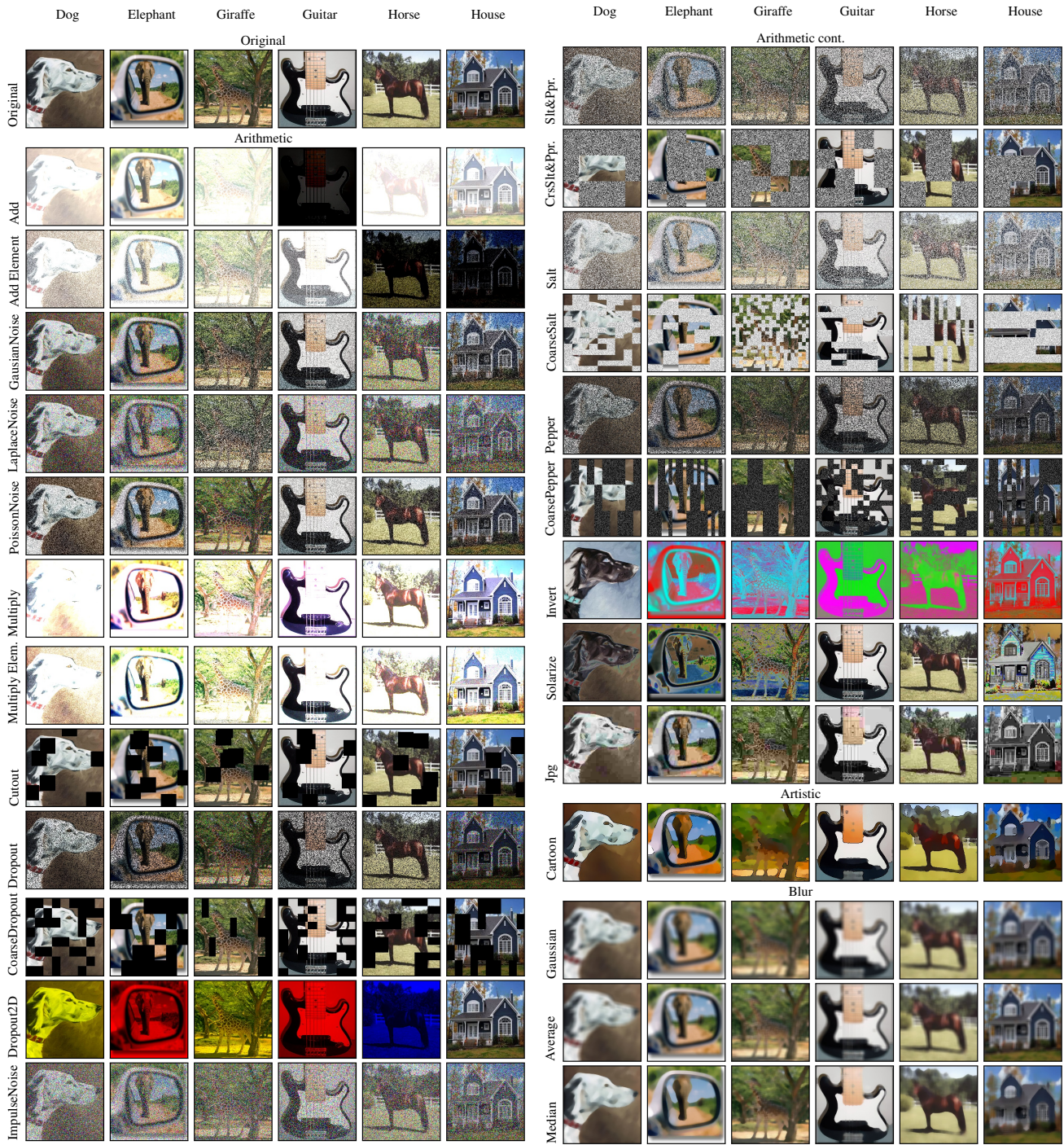


Figure 13. Examples of augmentations used from each augmentation category.

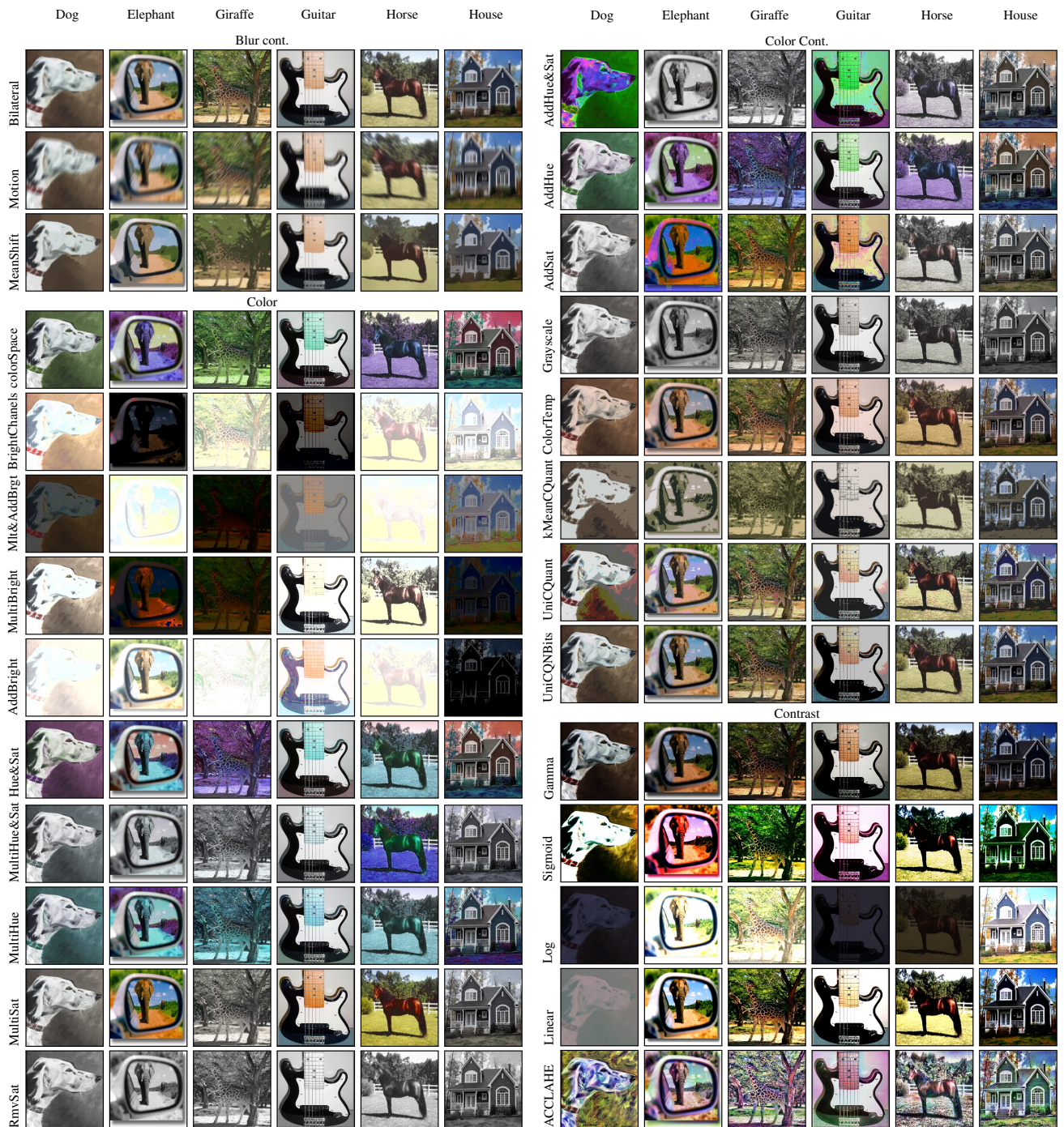


Figure 14. Examples of augmentations used from each augmentation category.

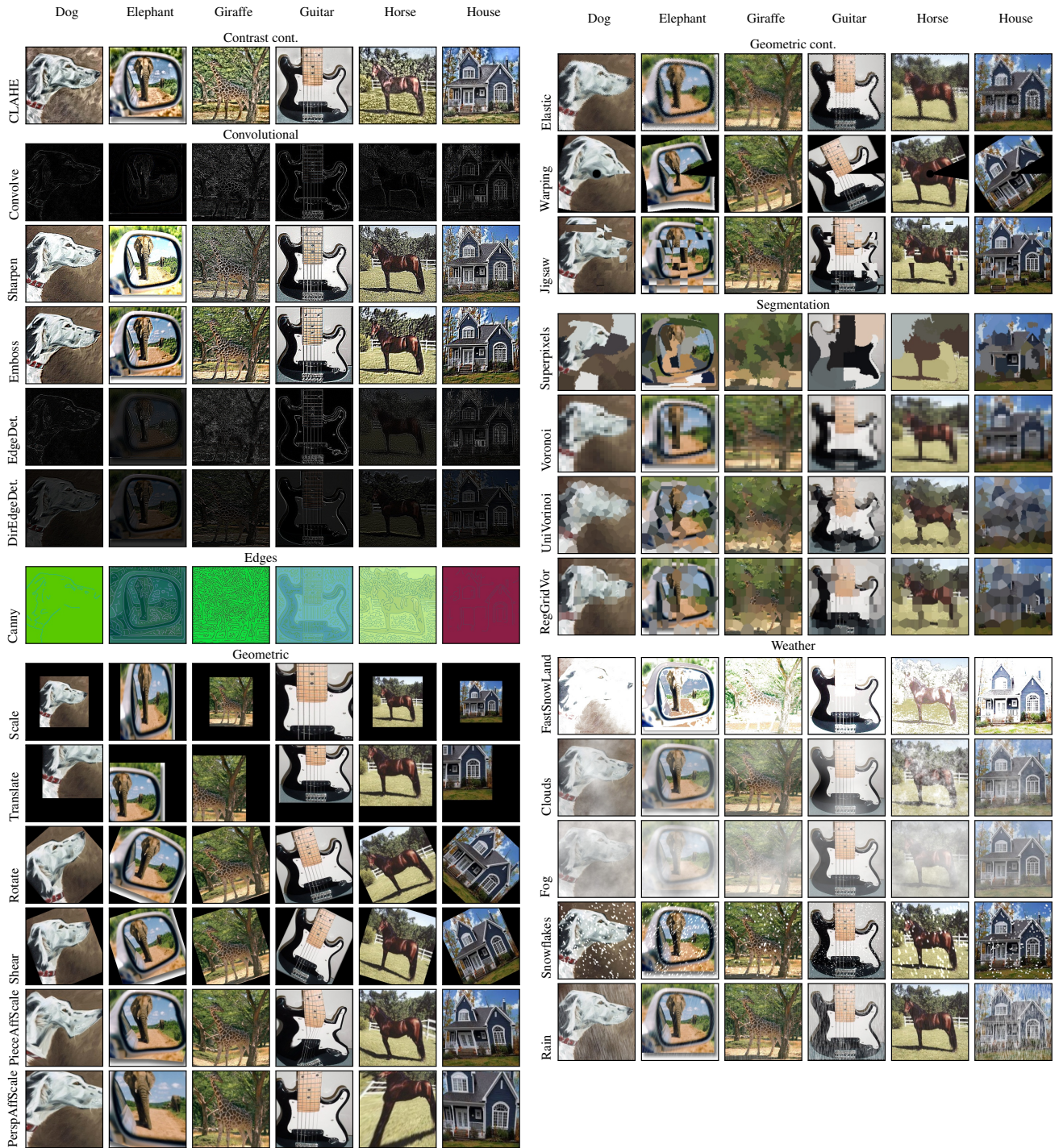


Figure 15. Examples of augmentations used from each augmentation category.